

Characterizing the Optical Response of Symmetric Hemispherical Nano-dimers

Tamara Attanayake¹ · Malin Premaratne¹ · Govind P. Agrawal²

Received: 9 January 2015 / Accepted: 20 April 2015
© Springer Science+Business Media New York 2015

Abstract We present the first comprehensive study of a hemispherical nano-dimer interacting with an optical field. We characterize the optical response of the hemispherical dimer numerically using the finite-element method. The qualitative insight gained through the numerical analysis is enhanced with a derivation of an analytical approximation for the polarizability of a symmetric hemispherical dimer by invoking the dipole-dipole approximation. The results explain the effects of inter-particle spacing and the polarization of external excitation on the extinction spectra. Considering three configurations of hemispherical dimers, we show that both the frequency and the strength of plasmon resonances in each configuration are highly dependent on the inter-particle distance and the state of polarization of the incident light. We also show that, in the case of longitudinal polarization and an edge-to-edge orientation, the hemispherical dimer provides much better near-field confinement and produces much more enhancement of the electric field than a spherical dimer of the same volume. This result should prove useful for sensing and SERS applications.

Keywords Dimers · Hemispherical · Plasmonics

✉ Tamara Attanayake
tamara.attanayake@monash.edu

¹ Advanced Computing and Simulation Laboratory (A χ L), Department of Electrical and Computer Systems Engineering, Monash University, Clayton, Victoria 3800, Australia

² The Institute of Optics, University of Rochester, Rochester, NY 14627, USA

Introduction

The astounding capability of nanoparticles in confining and enhancing applied optical fields of certain frequencies has attracted a considerable attention of researchers over the last few decades [1]. This phenomenon, which resulting from coherent oscillations of surface electrons in the presence of an external electromagnetic field, has found applications in diverse fields varying from bio-optics to nanophotonics [2–5]. With the advancements of nano-fabrication methods and plasmonic theories, the growing interest in integrating nanoparticle ensembles has led to variety of stable nanoparticle structures ranging from nanosphere to nanomatryushka configurations [4–7]. However, despite its simplicity, the hemispherical shape of nanoparticles is rarely employed in plasmonics applications. Here, we are highlighting the main characteristics of such dimers so that researchers may adopt it for nanophotonic applications.

When nanoparticles are arranged closely, plasmon modes of solitary particles interact with each other, causing optical effects that significantly differ from their solitary complements. Properties of such interactions can be tuned by varying the size, shape, geometrical arrangement, spacing, and excitation direction to realize a specific behavior of interest [5, 6, 8]. Indeed, in many novel applications of nanophotonics, an ensemble of nanoparticles are manipulated to obtain a variety of characteristics such as frequency shifts, splitting of resonance modes, and field enhancements [5, 8, 9].

The interaction of an electromagnetic field with nanoparticles is often modeled using quasistatic approximation owing to its capability of predicting results with high accuracy and adequacy for a wide range of nanoparticle ensembles [10, 11]. The theory assumes that the time-dependent electromagnetic field has a constant phase throughout the

nanocluster, and thus provides a simplified analytical solution for structures with dimensions considerably shorter than the wavelength of the incident field. When the size of a particle becomes comparable to electron's mean free path, electron-surface scattering and spatial dispersion of the dielectric function increase and become non-negligible with respect to inherent bulk collision frequency [12, 13]. For a more rigorous investigation, one must take into account for these effects using nonlocal or quantum theories [7]. Since such effects become crucial only for dimensions below 5 nm, classical theory based on Maxwell's equations can be used for larger dimensions provided material properties are taken into account through experimentally measured bulk permittivity or through the Drude model with appropriate parameters [14].

The mutual interaction between localized surface plasmon resonances of nanoparticles placed in proximity can be explained with a well-established model based on a molecular hybridization process, as pioneered by groups of Nordlander [8, 15] and El-Sayed [5]. By mimicking two atoms combined to form a molecule, it was predicted that plasmon modes of two closely spaced nanoparticles undergo either in-phase or out-of-phase coupling to form new resonance modes. The technique has shown good agreement with experimental data obtained for various shapes of nanoparticles [16–18]. Nonetheless, numerical simulations are generally required to identify and explain salient features associated with different geometries. Computational techniques, such as the finite-difference time domain method, the discrete dipole approximation, the finite element method (FEM), and the finite integration technique, are imperative in this realm [19–22].

In this article, we report on a comprehensive analysis of hemispherical dimers. We study two vertically aligned arrangements and one horizontal arrangement such that all of them are symmetrical to the x - z plane. We first derive the orientation and polarization-dependent polarizability of the dimer in the quasistatic approximation using the dipole-dipole interaction model (DDIM). We then use it to obtain analytical expressions for the absorption and scattering cross sections. By analyzing the results of the analytical model and the numerical simulations based on the finite element method, we show that optical properties of hemispherical dimers are highly dependent on the polarization of the incident field, the inter-particle separation, and the geometrical configuration. In all nanoclusters that we studied, the plasmon resonance shows a profound shift to lower frequencies as the junction becomes narrower when the field is polarized parallel to the junction. On the other hand, in the case of orthogonal polarization, change in the frequency of the plasmon resonance is in the opposite direction and its magnitude is much smaller com-

pared to the parallel polarization case. This behavior can be attributed to the better coupling between plasmon modes in the case of parallel polarization. By comparing the results obtained with the two methods, we demonstrate that the DDIM projections are sufficiently precise for wide gaps, but fail in identifying salient orientation dependent features for smaller separations.

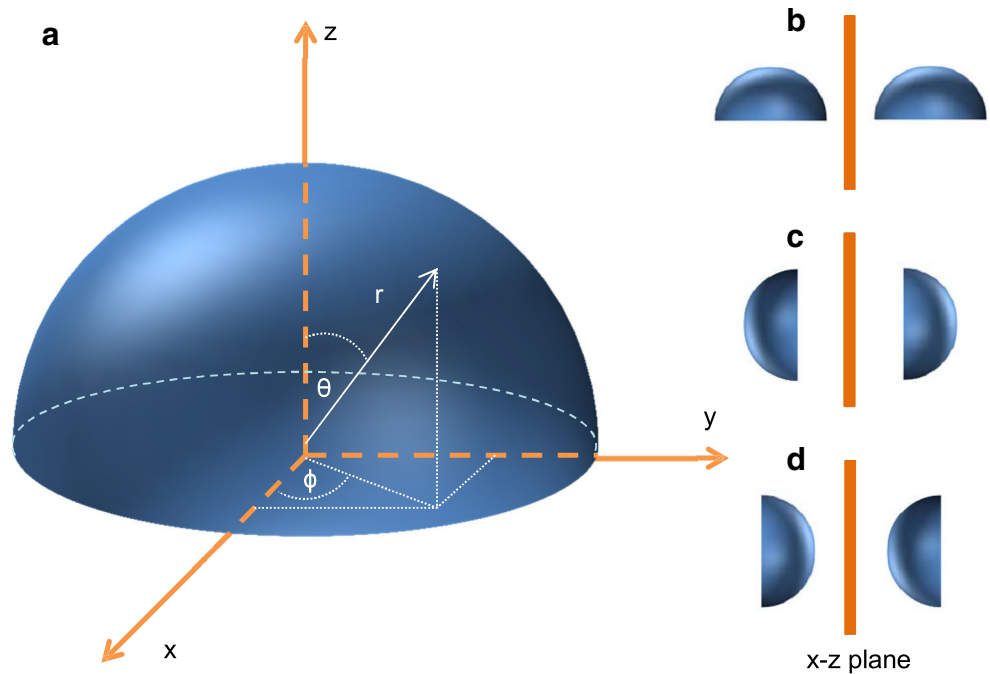
Among all the cases that we studied, the largest frequency shift and field enhancement in the junction were observed in the edge-to-edge orientation for parallel excitation when the nanoparticles were separated by 2 nm. Indeed, the electric field enhancement factor in the above configuration was larger than that of an equal volume spherical dimer with the same gap and polarization. Our results suggest that the simple hemispherical-shape nanocluster studied here would be highly useful for surface enhanced Raman scattering (SERS) and other sensing applications. Moreover, we show that rounding of hemisphere edges does not affect the qualitative behavior of interacting plasmon modes in the dimer, although such a rounding produces quantitatively non-negligible effects.

Orientation-dependent Polarizability of Hemispherical Dimers

To elucidate the dependence of optical characteristics on hemisphere orientation, we primarily consider three configurations shown in Fig. 1. In part (b), we illustrate the edge-to-edge configuration. In the case of side-by-side orientation, we study two cases. In one case shown in part (c), flat surfaces of hemispheres face each other (D' - D orientation), while in the second case shown in part (d), spherical surfaces face each other (D - D' orientation). The following analysis is limited to structures symmetrical to the x - z plane. The nanoensembles with inclinations in between are not studied here. Also, hemispherical dimers with size and composition disparity are beyond the scope of the paper. We first find the polarizability of a single hemisphere and then approximate the interaction of plasmon modes associated with two hemispheres using the DDIM.

In previous attempts on calculating the dipole moment of a hemispherical nanoparticle [23, 24], the potential was expressed in spherical harmonics, limiting the range of polar angle θ from 0 to 90° in applying boundary conditions (see Fig. 1a). However, due to the sharp termination of the curved surface at the base of the hemisphere, spherical harmonics are an imperfect basis to model hemispheres [25]. Their use requires a large number of base terms in the potential expansion, which increases computational complexity [23]. Here, we consider hemispheres with rounded edges and follow the method used by Kettunen et al. [26] to derive

Fig. 1 **a** Geometry and the notation used for a hemisphere-shape nanoparticle. **b–d** Three dimer arrangements symmetrical to the x – z plane that were analyzed in our study



the polarizability. This method provides a simple approach to get analytical expressions for shapes with rotational symmetry such as spheres, cylinders, and hemispheres. With this approach, we solve Maxwell’s equations, both analytically and numerically, with the quasistatic approximation.

Polarizability of a Single Hemisphere

In deriving the polarizability of a single hemisphere, we assume the particle to be oriented symmetrically around the z axis, as illustrated in Fig. 1. For a particle placed in a source-free electric field, the scalar potential satisfies the Laplace equation [27],

$$\nabla \cdot \mathbf{D} = \nabla \cdot [\varepsilon(-\nabla\phi)] = 0, \tag{1}$$

where \mathbf{D} is the electric displacement field, while ε and ϕ represent the permittivity and the scalar potential, respectively. The potential inside and outside the particle is denoted as ϕ_{in} and ϕ_{out} , respectively. The latter can be expressed in spherical coordinates (r, θ, φ) as

$$\phi_{out}(r, \theta, \varphi) = \phi_0 + \frac{P(r, \theta, \varphi)}{4\pi \varepsilon_0 a^2}, \tag{2}$$

where ϕ_0 is the excitation potential that relates to applied electric field E_0 as $E_0 = -\nabla\phi_0$ and P represents the dipole moment of the hemisphere. Furthermore, ε_0 and a denote the permittivity of free space and the distance from the center of the hemisphere, respectively.

In solving Eq. (1) for ϕ_{in} and ϕ_{out} separately, symmetric properties of the hemispherical geometry were employed. Since the hemisphere is placed with a rotational symmetry around the z axis, the potential functions can be separated as

$$\nabla\phi(r, \theta, \varphi) = \phi(r, \theta)\phi'(\varphi), \tag{3}$$

and the Laplace equation can be simplified by using the cylindrical coordinates ρ and z as

$$\frac{\partial}{\partial\rho} \left(-\rho\varepsilon \frac{\partial}{\partial\rho} \phi(\rho, z) \right) + \frac{\partial}{\partial z} \left(-\rho\varepsilon \frac{\partial}{\partial z} \phi(\rho, z) \right) + \frac{\varepsilon}{\rho} \phi(\rho, z) = 0. \tag{4}$$

This simplified equation can be written in the form of the following Helmholtz equation:

$$\nabla \cdot (-c\nabla u) + au = f, \tag{5}$$

where the coefficients c, a, f are obtained from Eq. 4.

Equation 5 was solved numerically with finite-element method (FEM), which was implemented utilizing the symmetry properties of hemisphere seen in Fig. 1a. This enhanced the accuracy of calculation by allowing the use of finer mesh, while maintaining a low computational complexity. Furthermore, since we are interested in the dipole effect of the nanoparticle, the boundary condition related to the continuity of the normal derivative of the background potential was defined in the far field. Therefore, in numerical simulations, the boundary of the host medium was set relatively far from the hemisphere boundary [26]. However, the background potential varies with the polarization

direction of the incident field and can be written as

$$\phi_{out_z}(r, \theta, \varphi) = -E_0 r \cos \theta + \frac{P \cos \theta}{4\pi \epsilon_0 a^2}, \quad (6a)$$

$$\phi_{out_x}(r, \theta, \varphi) = -E_0 r \sin \theta \cos \varphi + \frac{P \sin \theta \cos \varphi}{4\pi \epsilon_0 a^2}, \quad (6b)$$

where ϕ_{out_z} and ϕ_{out_x} are the scalar potentials corresponding to the short axis (z axis) and the long axis (x axis) polarizations. The far field boundary was taken as spherical in shape with a radius of R' . Hence, the normal derivative of these potentials can be obtained by taking partial derivative with respect to r and this can be further simplified as

$$\frac{\partial}{\partial r} \phi_{out_z}(r, \theta, \varphi) = -\frac{2}{r} \phi_{out_z}(r, \theta, \varphi) - 3E_0 \cos \theta, \quad (7a)$$

$$\frac{\partial}{\partial r} \phi_{out_x}(r, \theta, \varphi) = -\frac{2}{r} \phi_{out_x}(r, \theta, \varphi) - 3E_0 \sin \theta \cos \varphi. \quad (7b)$$

Adhering to the symmetry of a hemisphere along the short axis, the boundary conditions to solve Eq. (4) can be then derived in cylindrical coordinates as [26]

$$\frac{\partial}{\partial n} \phi_{out_z}(\rho, z) = -\frac{2}{R'} \phi_{out_z}(\rho, z) - \frac{3E_0}{R'} z, \quad (8a)$$

$$\frac{\partial}{\partial n} \phi_{out_x}(\rho, z) = -\frac{2}{R'} \phi_{out_x}(\rho, z) - \frac{3E_0}{R'} \rho, \quad (8b)$$

where \mathbf{n} is the unit vector normal to the boundary. These equations can be implemented using finite element method with the ‘‘Flux/Source’’ boundary condition

$$-n \cdot (-c \nabla u) = g - qu. \quad (9)$$

The preceding set of equations were solved numerically for frequencies ranging from 450 to 900 THz in 2 THz steps. The dipole moment along the axis of interest for each frequency was then obtained by the volume integration of the polarization along that axis. The dipolar polarizability; α is related to the dipole moment as

$$p = \epsilon_0 \epsilon_m E_0 \alpha, \quad (10)$$

where ϵ_m represents the host medium relative permittivity.

Polarizability of a Hemispherical Dimer

In the case of a dimer, the electric field experienced by one particle is modified by the field originated from the induced potential of the other particle. Therefore, the polarizability of one particle depends not only on the external perturbation but also on the scattered electric field of the neighboring particle. To include these effects, we employed dipole-dipole interaction theory, which is known to be accurate for sub-wavelength structures when separation between particle is on order of a particle size or higher [28, 29]. In this framework, induced dipole of the hemisphere is approximated to

a point dipole placed in the center of the nanoparticle. As a result, the electric fields on two hemispheres i and j placed in proximity can be expressed as,

$$E_i = E_0 + \frac{P_j}{4\pi \epsilon_0 \epsilon_m |\mathbf{r}_i - \mathbf{r}_j|^3} \beta \quad (11a)$$

$$E_j = E_0 + \frac{P_i}{4\pi \epsilon_0 \epsilon_m |\mathbf{r}_i - \mathbf{r}_j|^3} \beta \quad (11b)$$

where P_i denotes the dipole moment and \mathbf{r}_i denotes the position of particle i , respectively (with same notations used for particle j). The orientation factor β reflects the effects of dipole direction on the polarizability [30] and takes the form

$$\beta = 3 \cos \theta_i \cos \theta_j - \cos(\theta_i - \theta_j), \quad (12)$$

where θ_i is the angle of the polarization vector for particle i from the inter-particle axis. The dipole moment of each particle can then be found using

$$P_q = \alpha_q \epsilon_0 \epsilon_m E_q, \quad (q = i, j), \quad (13)$$

where α_i being the polarizability of the particle i . Seeing that the total dipole moment of the system is $P_i + P_j$, the polarizability of the hemispherical dimer can be obtained from

$$\alpha_d = \frac{P_i + P_j}{\epsilon_0 \epsilon_m E_0}. \quad (14)$$

Since our study is limited to identical hemispheres, $P_i = P_j$ and Eq. (14) can be simplified as

$$\alpha_d = \frac{2\alpha}{1 - \alpha F}, \quad (15)$$

where we have introduced

$$F = \beta / [4\pi \epsilon_0 |\mathbf{r}_i - \mathbf{r}_j|^3]. \quad (16)$$

Once the polarizability of the composite is determined, absorption and scattering cross sections for various orientations and polarizations of the incident field are obtained using [31]

$$C_{\text{abs}} = \frac{2\pi}{\lambda \epsilon_0} \text{Im}(\alpha_d), \quad C_{\text{sct}} = \frac{8\pi^3}{3\pi \epsilon_0^2 \lambda^4} |\alpha_d|^2. \quad (17)$$

The extinction cross section of hemispherical dimer is then given by

$$C_{\text{ext}} = C_{\text{abs}} + C_{\text{sct}}. \quad (18)$$

Numerical Modeling for Symmetric Hemispherical Dimers

The response of the hemisphere ensembles to an external electromagnetic field was simulated numerically with FEM

using CST microwave studio frequency domain analysis [21]. The integration domain was in the form of a three-dimensional box containing one or more nanoparticles inside it with a symmetry to the x - z plane. Hemispheres with a radius of 20 nm were used in our calculations while the inter-particle distances were varied from 2 to 50 nm. Also, a rounding radius of 3 nm was employed for comparing simulated results with theoretical observations. The size of the box was changed according to the orientation of hemispheres and the direction of field polarization, to minimize reflection or scattering at the box boundaries. A tetrahedral mesh was employed for discretization because it models rounded shapes more accurately than a hexahedral mesh [32]. Furthermore, the size of elementary cell was kept the same in all simulations for proper comparison. We took full advantage of the electric and magnetic field symmetries in accordance with the polarization direction to reduce the computational complexity.

Noble metals are often used as plasmonic materials as their plasmon modes fall in the visible frequency range [1]. The reason is that localized surface plasmon resonances are only viable in materials with a large negative value of the real part of the dielectric function such that $-\text{Re}[\varepsilon] \gg \text{Im}[\varepsilon]$, a condition satisfied by noble metals. Among gold, silver, copper, and aluminium, we chose silver for our analysis since we found that it was possible to excite a broad range of frequencies and obtain higher electric field enhancement for hemispherical dimers in the case of silver. The complex dielectric function of the nanoparticles was obtained from experimental data of Palik [33], and a fourth-order interpolation technique was used to derive dielectric functions for frequencies that were not available in the data. In all cases, unless specified otherwise, we considered the background material to be air and set the host medium permittivity as one.

We illuminated the dimer with plane waves of similar frequencies that were used in analytical model and calculated various optical properties for the longitudinal and transverse polarizations of the electric field. The polarization that was parallel to the line connecting centers of the hemispheres was defined as longitudinal, or parallel polarization, while transverse polarization was considered to be normal to this axis. Numerical results for absorption, scattering and extinction cross sections were obtained by setting up the near field and far field monitors for each excitation frequency.

Orientation-Dependent Extinction Properties of Nano-hemispherical Dimers

Before discussing the results for a hemispherical dimer, we first briefly consider the major plasmon modes of a single hemisphere. Figure 2 shows the extinction spectra of

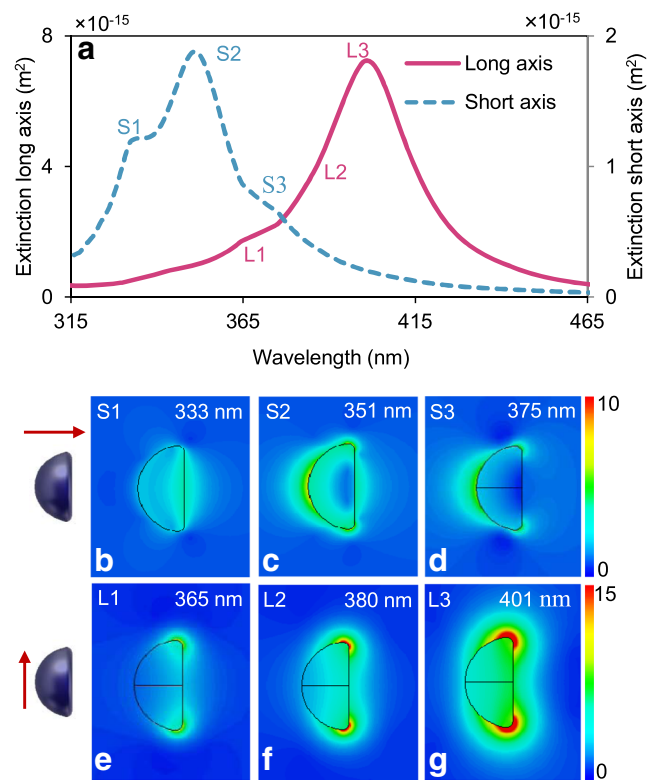


Fig. 2 **a** Polarization-dependent extinction cross section of a single hemisphere as a function of excitation wavelength. The plasmon resonance modes resulting from short and long axis excitation are marked as S1, S2, S3, and L1, L2, L3, respectively. **b–g** Snapshots of electric field profiles for these six plasmon mode. The arrows indicate the polarization direction

a single hemisphere for polarization along the long and short axes, respectively. In the long-axis case, the maximum occurs at 401 nm, while slight shoulder-like features (marked L1 and L2) occur at 365 and 380 nm, respectively. These plasmon modes result from dipole oscillations of bound electrons located primarily in the corners of the hemisphere. When the excitation is along the short axis, three substantial plasmon modes can be identified (marked as S1, S2, and S3) at 333, 351, and 375 nm, respectively. As seen from the electric field profiles, the short-wavelength resonance S1 is a consequence of the dipole oscillation which is oriented along the short axis, while S2 and S3 are split dipoles for which electron concentration is primarily on the edges of the hemisphere.

Generally, the addition of a new particle boosts the total extinction of a composite. When new particles are included, the absorption strength of the ensemble dramatically amplifies due to increase in number of electrons, which facilitate enriched coupling with electromagnetic energy [8]. Furthermore, nanoensembles have larger surface areas than solitary particles thus receive an enhanced contribution from the scattering cross section. However, the absorption dominates over the scattering in small nanoclusters, hence effect of

the former is profound [34]. The tunneling of electrons between nanoparticles was found to be negligible for junction widths larger than 0.5 nm and is not considered in our analysis [35].

Figure 3 shows the extinction cross section of nanoclusters containing hemispheres of 20 nm radius and assembled in edge-to-edge configuration for different inter-particle distances. Extinction spectra of a single hemisphere is also shown as a dotted line for comparison. With the addition of the second particle, plasmon modes of individual particles interact with each other, resulting in new resonance modes. Analogous to the various shapes of nanoparticle dimers [16, 36–38] studied before, the coupling process of a hemispherical dimer in parallel polarization (Fig. 3a) mainly depends on the inter-particle distance d , as evident by the prominent shifts in the extinction spectrum for various gaps compared to that of a single particle. When d is large (order of the hemisphere radius or more), the interaction between plasmon modes becomes weak, thus resulting in minor frequency changes. Nevertheless, only the L3 resonance mode appears to be involved in hybridization, while the weak edge modes at 365 and 382 nm are not strong enough to interact effectively, as manifested by unchanging resonance values for the dimer.

In the case of transverse polarization (Fig. 3b), the resonance peak exhibits a blue shift as the inter-hemisphere gap is reduced. The change of frequency is very small, and

the extinction spectrum is essentially a linear superposition of the single-hemisphere spectra. These characteristics of the hemispherical dimer can be understood by the diagrams shown in Fig. 3c, d for parallel and transverse polarizations, respectively. In the dipole-coupling model, hybridization of individual plasmon modes removes the degeneracy for both polarizations, resulting in higher and lower energy components. In the case of parallel polarizations, the orientation of individual plasmon modes are in-phase, and induced charges on each particle at the edge facing the junction are opposite to each other. For instance, in the lowest branch of Fig. 3c, negative charges of the left hemisphere are facing positive charges of the right hemisphere. The attraction between these charges decreases the restoring force created by solitary particles against an external field, reducing the resultant resonance frequency [39]. With a lowering of spatial separation, this attraction increases further and the resonance frequency shifts to even longer wavelengths. On the other hand, in the anti-bonding situation, individual dipole moments are oriented out-of-phase with each other, hence the reaction in the junction is repulsive and supports to the restoring force. Therefore, the plasma resonance frequency of the dimer increases. However, in symmetric dimers, these equal and opposite dipole moments get canceled and are not visible in spectral diagrams [8]. Similarly, in the case of transverse excitation of a symmetric dimer, both bright and dark modes are possible. However, as seen from Fig. 3d, the

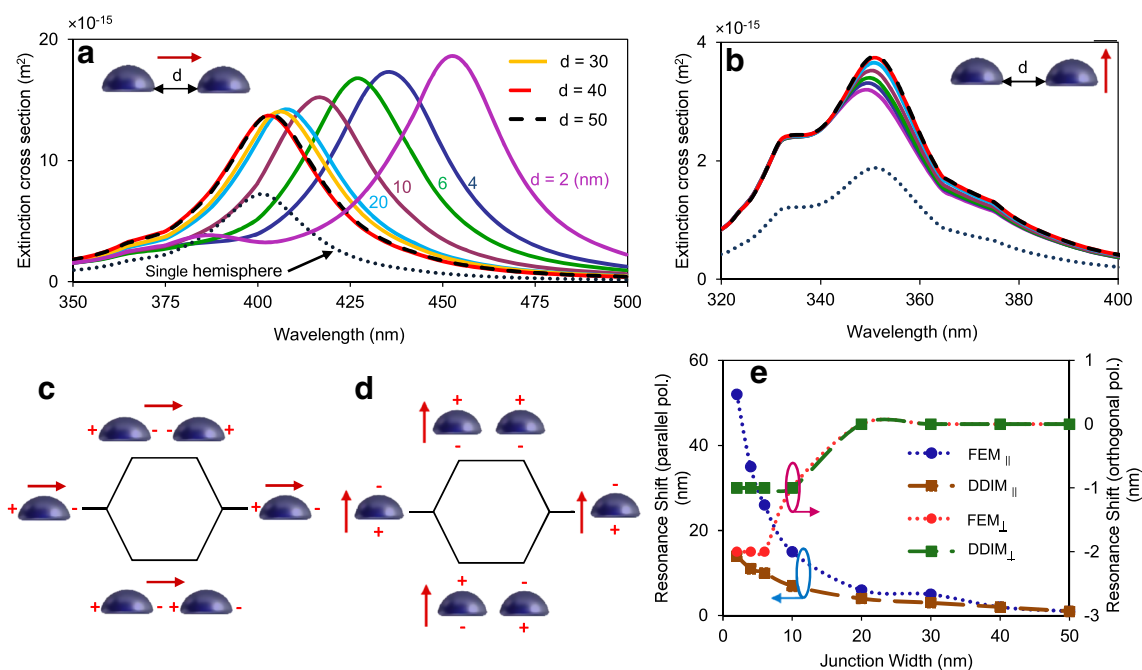


Fig. 3 Simulated extinction spectra for edge-to-edge configuration with **a** parallel and **b** transverse polarizations for different inter-hemisphere separations d . Schematic diagrams illustrating the hybridization phenomenon, respectively, for **c** parallel and **d** transverse

polarizations. **e** Comparison of resonance peak shifts obtained from DDIM with FEM simulations for various junction widths. *Horizontal and vertical arrows* indicate parallel and transverse polarizations, respectively

in-phase interaction is repulsive here, therefore we can only observe a distinct blue shift in the extinction spectrum when the separation distance is reduced. The change of frequency in this polarization is much smaller in compared to parallel polarization due to weak interaction between the charges that are relatively far apart.

The Fig. 3e illustrates a comparison of the plasmon resonance shift obtained from the numerical simulations and the analytical model in terms of junction width. In the case of parallel polarization, the displacement of resonance peak estimated from simulations shows an almost exponential variation with the junction width. This is consistent with the results obtained for dimers of other shapes (such as nanoprisms [36], nanorods [16], nanospheres [37], and nanoshells [38]) calculated using different methods. However, predictions of the analytical model diverge considerably from simulation results for small junction widths ranging from 2 to 20 nm. This is apparent from a 38 nm difference between the projected displacements of two methods for 2 nm inter-particle distance. The main cause behind this behavior is the higher separation of dipoles in the analytical model [16]. Nevertheless, both results converge when the separation is increased, coinciding for inter-particle distances greater than 40 nm. Note that the agreement is much better in the case of orthogonal polarization. The analytical and numerical results agree when the separation is 10 nm or more, and the difference for shorter separations is around

1 nm. Since the dipoles are far apart from each other for this polarization, the point dipole approximation is much more relevant for orthogonal polarization compared to parallel excitation.

Extinction properties in the case of the second configuration in which the hemispheres are placed side-by-side are illustrated in Fig. 4. In part (a), where results are shown for D'-D orientation, the S1 plasmon mode shows a strong hybridization, moving the resonance frequency from 333 nm at an inter-particle distance of $d = 50$ to 346 nm at $d = 8$ nm, and then to 354 nm at $d = 2$ nm. The coupling of the S2 mode is much weaker compared to the S1, while the S3 mode is not involved in hybridization at all, resulting no change in the plasma resonance frequency. As seen from Fig. 2c, the field distribution of the S2 is mainly concentrated in outer spherical region and edges. Whereas, in the case of S1 mode, concentration is high along the flat surface and is spread towards the neighboring particle. Therefore, even though S2 is the dominant plasmon mode for a single hemisphere, coupling is stronger for the S1 mode in the case of a D'-D ensemble, consequently possessing a larger red shift. For smaller separations, the change of the S1 becomes excessive and interferes with the hybridized S2 mode, featuring an enhanced extinction. With further reduction of the spatial gap, spectrum of the hemispherical dimer converges to that of a single sphere of the same radius. This spectrum is calculated with Mie theory and shown

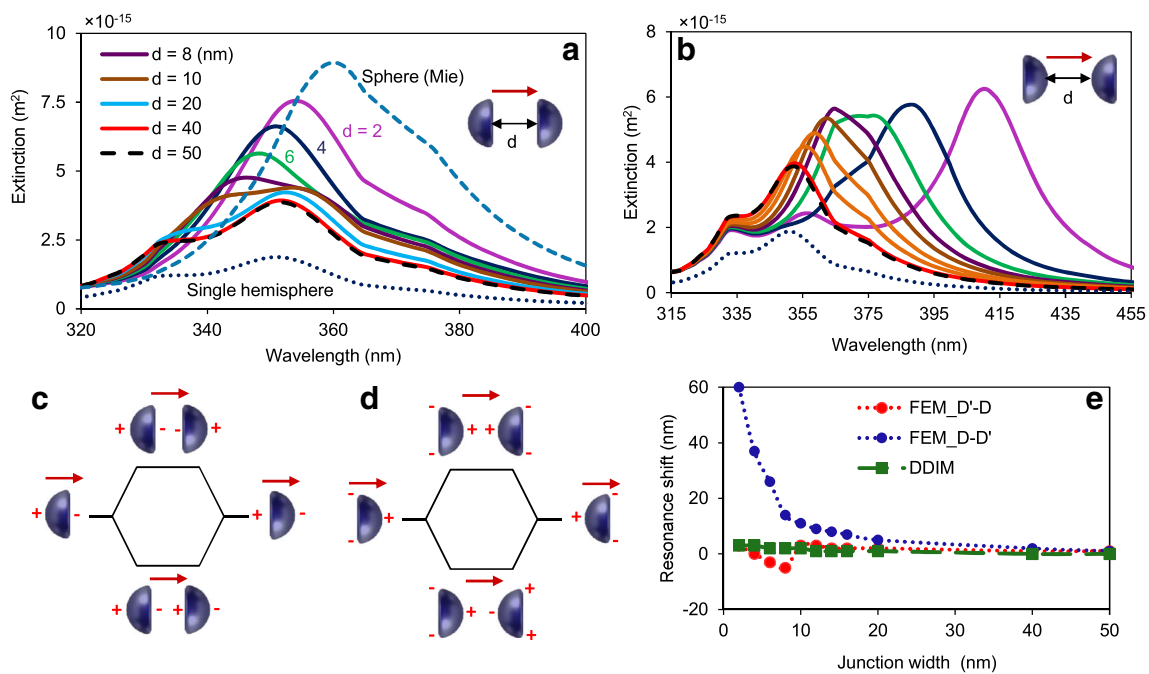


Fig. 4 Longitudinal excitation on two side-by-side configurations in which extinction cross section dependency on spatial gap d is shown in (a) for D'-D and (b) D-D' orientations. Orientation-dependent coupling process based on DDIM model for (c) D'-D and (d) D-D',

when an external perturbation is applied in the direction of arrows. e Comparison of DDIM and numerically predicted resonance peak position change as a function of spatial gap

by a dashed blue line in Fig. 4a, assuring the accuracy of simulated results.

In the second D-D' case shown in Fig. 4b, the S1 mode does not interact as the E-field is confined to the outer region, and linear superposition of plasmon modes occurs at 333 nm. Similarly, for all distances, resonance at 375 nm is invariant in terms of frequency and coincides with solitary particle condition. From Fig. 2, it can be seen that the S3 mode is the weakest peak in the case of short-axis polarization; thus, even though the field distribution is high along the spherical side, it is not strong enough for the interaction to occur. In contrast, the coupling of S2 mode is strong for short separations, and it moves the resonance peak from 351 to 411 nm for a 2 nm separation, causing a 60 nm shift. The main cause behind such a large frequency shift is (i) the large concentration of electric field lines at the junction and (ii) the high intensity of mode S2, which paves the path to an enhanced plasmon interaction. Consequently, when compared to the D'-D orientation, magnitudes of the resonance peaks are quite similar in spite of a large shift. Parts (c) and (d) of Fig. 4 show, respectively, the hybridization process of the S1 mode in D'-D orientation and of the S2 mode in D-D' orientation. Analogous to the edge-to-edge configuration, the in-phase oscillation results in low energy in both

cases, resulting a red-shifted hybrid mode, while the higher-energy antisymmetric mode gets canceled out due to the symmetry of the ensemble. Also, shifts and amplitudes are much lower here than the edge-to-edge configuration, which can be attributed to a lower dipole moment due to shorter displacement of surface electrons.

Changes in the resonance frequencies calculated with the DDIM method and the FEM simulations for the two side-by-side configurations are shown in Fig. 4e. As the polarization of a single hemisphere is manifested by a point dipole, this method fails in capturing distinct orientation-dependant behavior for shorter separations. This is evident by nearly 20 times more displacement predicted by the FEM results compared to the 3 nm shift projected by DDIM for 2 nm gap in D-D' orientation. From Fig. 4a, it is evident that the peak of the hybridized S1 mode becomes more prominent than the S2 mode for junction widths lower than 10 nm. This feature moves the resonance maximum to higher frequencies from $d = 8$ to 4 nm, and then as a consequence of red shifting of S1, the peak moves back to lower frequencies. This behavior is seen in Fig. 4e, where red dotted line shows a sudden dip and then coincides with DDIM results for a $d = 2$ nm gap. Even though the projected shift is the same for both methods in the case of lowest separation, the

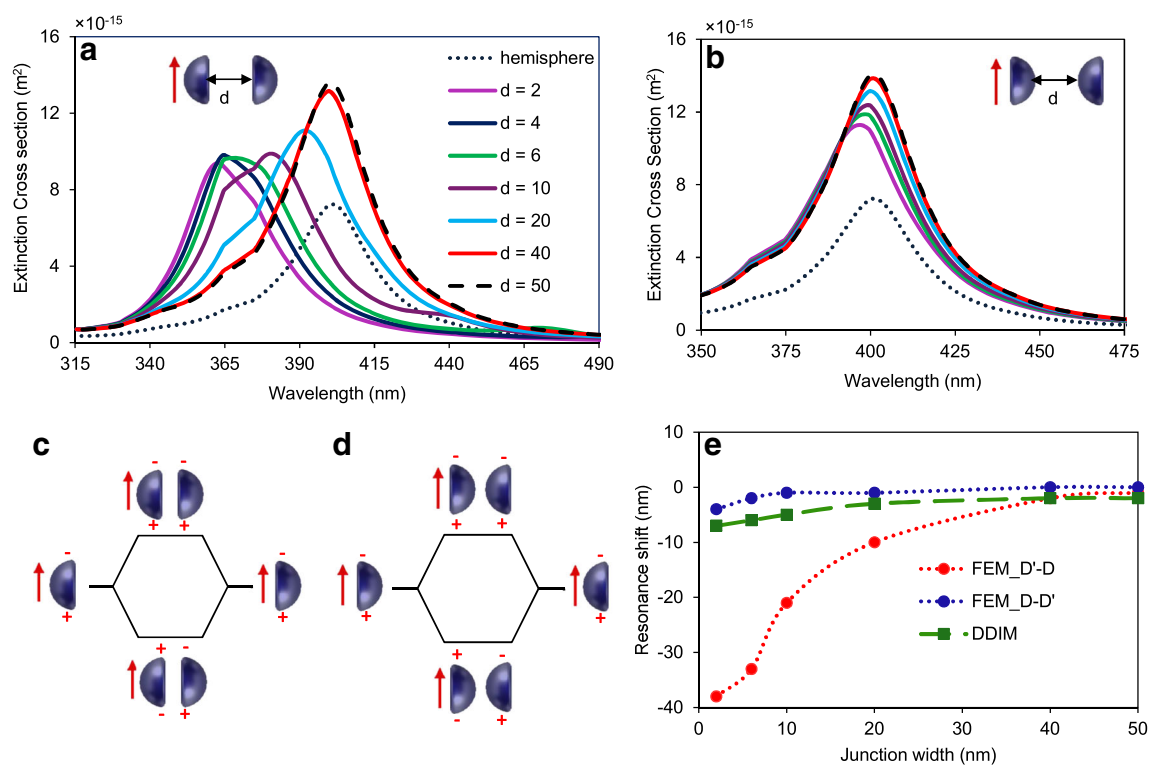
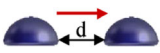
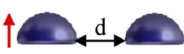
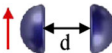
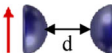


Fig. 5 Extinction cross section as a function of excitation wavelength for **a** D'-D and **b** D-D' arrangements when incident light is polarized orthogonal to the axis connecting centers of hemispheres (indicated by an arrow). Schematic diagrams showing plasmon hybridization for

c D'-D and **d** D-D' orientations. **e** Results obtained from DDIM and FEM simulations are analyzed based on resonance peak shifts as a function of junction width d

Table 1 Separation-dependant resonance properties of hemispherical dimers

Configuration	Resonance peak shift	Validity of DDIM
	Pronounced red shift as the gap becomes narrow	Larger difference for smaller gaps
	Slight red shift	Mostly consistent with simulations
	Larger red shift but lower than first configuration	Error increases exponentially for narrow gaps
	Slight blue shift	Consistent with simulations
	Pronounced blue shift for narrow gaps	Large errors as gap narrows
	Minor blue shift	Agrees with simulations

peak of $D'-D$ results from the superposition of red shifted S1 and S2 modes, while that for DDIM results from only the coupled S2 mode. Nevertheless, the location of resonance frequency is quite accurate for up to $d = 10$ nm separation in the $D'-D$ case, whereas it starts deviating from $d = 20$ nm in the case of $D-D'$. However, both simulation results are in good agreement with the analytical model for larger distances because the point dipole approximation becomes accurate for such large values of d .

In the case of transverse polarization, extinction spectra are quite similar in both side-by-side orientations when junction width is relatively large (Fig. 5). With the reduced separation, the $D'-D$ configuration shows a profound blue shift, whereas changes in the frequency for $D-D'$ are fairly small. Since the electric field lines are gathered at the edges of the hemisphere for long-axis excitation, the probability of having hybridized plasmon modes is higher in the former case. Nevertheless, as illustrated in Fig. 5a, the coupling only occurs for the L3 plasmon mode, which has the highest field concentration, and the resultant plasmon mode moves to higher frequencies. Since the gap between the L1, L2, and L3 modes are minor (of around 20 nm), the blue shift of the 401 nm peak gets added to high-frequency modes. Because of this interference, spectral width first increases with lowering of the separation and then drops again for shorter gaps when the resonance shift is higher than the gap between the original modes. On the other hand, in the $D-D'$ orientation, the electric field intensity is less in the junction, and a small blue shift is visible in the extinction spectrum.

The hybridization diagrams in Fig. 5c, d explain the movement of plasma resonance frequencies for this

polarization. Similar to previous results for edge-to-edge transverse excitation, the hybridized plasmon modes get blue shifted owing to the presence of repulsive charges in close proximity. This change in the resonance peak position is highly orientation dependent, as evident from Fig. 5e, which shows a significant deviation of $D'-D$ in comparison to $D-D'$. Nonetheless, unlike the short axis excitation, DDIM predictions are compatible for $D-D'$ orientation for all distances. As was explained above, the field concentration is low on the junction side, thus the plasmon modes are far apart in $D-D'$, resembling the point dipole in the DDIM. However, the coupling of high-intensity L3 modes causes an eccentricity of simulated results from the DDIM estimation for $D'-D$ orientation. A summary of changes in the resonance frequency with the inter-hemisphere distance predicted by the numerical simulations and comments on validity of the analytical method is presented in Table 1.

Our results indicate that the extinction spectra of a hemispherical dimer exhibit improved characteristics compared to a spherical dimer of the same volume. A comparison of the resonance peak shift in the cases of hemispherical and spherical dimers is shown in Fig. 6 as function of the spatial gap. The analysis was performed for hemispherical dimers with radii 20 and 40 nm, and in each case we studied the behavior of spherical dimers with either equal volume or radius. The change in resonance frequency was calculated by comparing it to the corresponding single-particle spectrum. In this study, we assumed that the hemisphere edges are not blended; the effect of blending is discussed later. The results show that the resonance shift is always higher for larger-size nanoparticles for all separations, irrespective of the shape of nanoparticles. In the case of particles with 40 and 20 nm radii, the dipole moment of the former is much larger than that of the latter because of an eightfold increase in its volume. When the dimer consists of particles

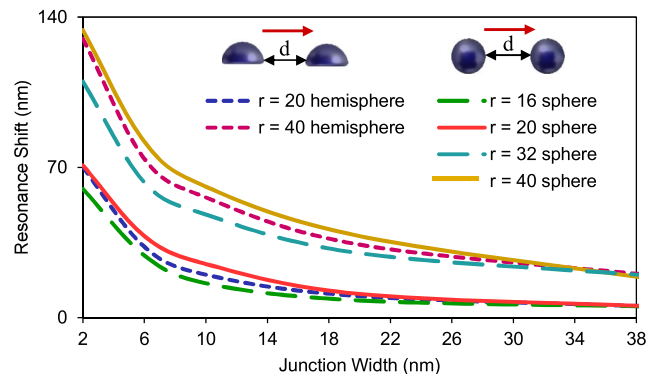
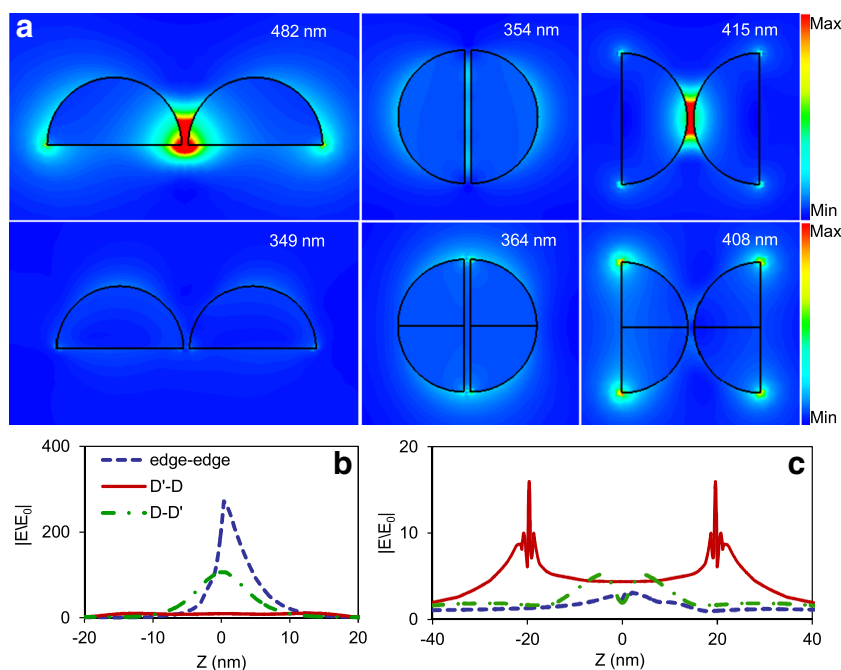


Fig. 6 Shift in the frequency of plasmon resonance as a function of junction width for hemispherical and spherical dimers when light polarization is parallel to the base of hemisphere, as indicated by arrows. Dashed curves are for hemispherical dimers with radii 20 and 40 nm; solid curves are for spherical dimers of different radii. In all cases, the inter-particle distance d is 2 nm

Fig. 7 **a** Electric field distribution in symmetric hemisphere orientations for parallel (*top row*) and orthogonal (*bottom row*) polarizations. Field enhancement factor along the *z* axis for **b** parallel and **c** orthogonal polarizations. In all cases, particles are separated by 2 nm



with higher dipole moment, it is clear from Eq. 11 that interaction between individual plasmon modes is much stronger, resulting in larger frequency shifts.

Let us compare the resonance shifts of a spherical dimer to a hemispherical dimer of equal radii. Even though the former’s volume is twice that of the latter, the resonance shifts are comparable. On the other hand, a comparison of equal volume dimers of two shapes reveals that hemispheres have better performance than spheres. For instance, in Fig. 6 40-nm-radii hemispheres exhibit a shift that is 20 nm larger compared to the spherical dimer for the lowest junction width. This behavior may occur for two reasons. First, since we consider particles with the same volume, the radius of the hemisphere is 40 nm, while that of the sphere is 32 nm. As charges can be displaced more in hemispheres, it is not surprising that their dipole moment is larger. Second, the concentration of the electric field lines near the edges of a hemisphere is more pronounced due to sharp boundaries (the lightning-rod effect). Since this feature increases the strength of the electric field, it improves the hybridization process. The main point to emphasize is that a hemispherical shape of dimers is likely to be more useful for chemical sensing applications [40–42].

Electric Field Enhancement of Hemispherical Nano-dimers

Electric field hot spots—areas with enhanced electric fields in nanoscale structures—have attracted considerable attention in recent years because of their applications in

surface-enhanced Raman scattering [43–45]. When metallic nanoparticles are placed in proximity, a dramatic enhancement of the local electric field occurs that can amplify weak Raman signals by many orders of magnitude, a phenomenon useful for the detection of single molecules. In the case of nano-hemispherical dimers, we find that the local field enhancement factor (defined as $F_E = |E|/|E_0|$) is strongly influenced by the orientation and interfacial separation.

Figure 7 presents the electric field profiles at the resonance peak for the three orientations considered in this paper when the inter-particle gap is 2 nm, a value for which maximum enhancement occurred. Top and bottom

Table 2 Summary of the orientation and polarization-dependent features of hemispherical nano-dimers based on Figs. 3, 4, 5, and 7

Configuration	Peak extinction		Peak Electric field enhancement factor
	Wavelength (nm)	Extinction (nm ²)	
	453	18,630	272
	354	7546	11
	411	6246	106
	351	3764	3
	400	13,604	16
	401	14,084	5

rows show the cases of parallel and transverse polarizations, respectively. Because of improved plasmon hybridization in the case of parallel excitation, the electric field intensity considerably increases in the junction region between the two particles. However, the first and third orientations in Fig. 7 show much larger values of F_E than the second orientation. The largest enhancement occurs for the edge-to-edge configuration with 272 times more electric field at the center of the gap compared to the incident field. On the other hand, the change of orientation to D-D' results in an enhancement factor of 106. This behavior is evident in Fig. 7b which shows variations of F_E along the z axis in the case of parallel excitation. The primary causes behind a large enhancement in the edge-to-edge configuration are its larger dipole moment and higher plasmon concentration. Despite the fact that the extinction cross section is nearly the same in both orientations of the side-by-side configuration (illustrated in Fig. 4), they have a huge difference in the field enhancement factor. The electric field is spread along the flat surface in the D'-D orientation, whereas field lines

are crowded in the top of the spherical surface in the D-D' case, consequently generating a larger electric field in the junction. In the case of transverse polarization, significant hot spots in the junction appear only near the edges in the D'-D orientation therefore, as seen in Fig. 7c, the field enhancement factor is fairly small compared to the parallel excitation.

The extinction cross section and electric field enhancement at the resonance peak are summarized in the Table 2 for all three configurations. In the case of parallel polarization, the peak cross section occurs for the lowest spatial gap, while it occurs when hemispheres are far apart in the case of transverse polarization. For this reason, we chose $d = 2$ nm and $d = 50$ nm for these two polarizations, respectively. Moreover, for spatial gaps from 2 to 50 nm, the maximum electric field in the junction is observed only for 2 nm; thus, the field enhancement factor is given only for this value.

Since the coupling between the plasmon modes is the strongest for the edge-to-edge orientation in the case of parallel (longitudinal) polarization, we used this orientation for

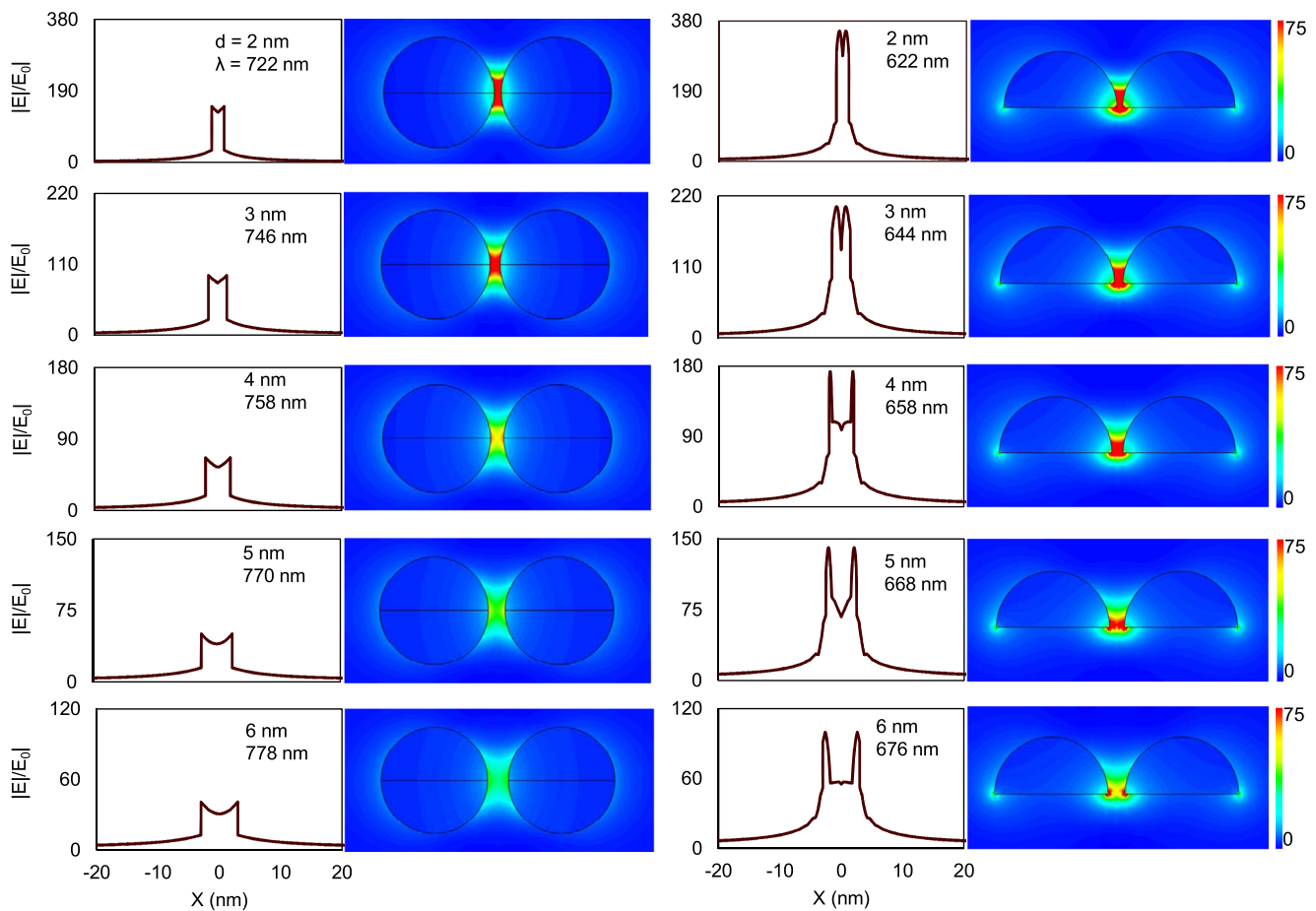


Fig. 8 Electric field enhancement factor variations along x -axis and electric field profiles for longitudinal polarization of equal volume spherical and hemispherical dimers as a function of the junction width. The resonance frequency and inter-particle distance are denoted by λ and d , respectively

comparing hemispherical and spherical dimers. We found that the field enhancement in the junction region is quite large for a hemispherical dimer compared to that of a spherical dimer of same volume. To elucidate this feature further, Fig. 8 shows the field enhancement factor and field-intensity profiles of spherical (two left columns) and hemispherical (two right columns) dimers for five different particle separations. In both cases, light frequency coincides with the frequency of extinction peak. In all electric field profiles, the ratio of maximum electric field compared to the incident field was kept at 75 to help comparison. Furthermore, as the nanoparticles with smaller dimensions provides higher field enhancement [46], we used hemispheres with 20 nm radius and spheres of equal volume.

It is evident from Fig. 8 that the field enhancement at the center of the junction is considerably higher for hemispherical dimers. More quantitatively, F_E for hemispheres with 2 nm spacing is twice that of spheres, and about 1.5 times larger for other spacings. These numbers agree with previous results obtained for similar arrangements of spherical dimers [47]. Note also that F_E at the center of the gap of a spherical dimer with 2 nm spacing is slightly lower than that of a hemispherical dimer with 3 nm spacing, and this pattern applies for other spacings as well. As explained earlier, such enriched properties of hemispherical dimers are a consequence of (i) their higher polarizability and (ii) the lightning-rod effect that results in intense coupling of the plasmon modes and much stronger electric-field enhancement. In our opinion, hemispherical dimers would provide better performance than spherical dimers when used for sensing and SERS applications. Analogues to the extinction properties, spacing between the two nanoparticles of a dimer also affects the field enhancement. As this spacing increases, the electric-field enhancement drops steeply. For example, the enhancement factor F_E drops from 272 for $d = 2$ nm to 98 for $d = 4$ nm to 55 for $d = 6$ nm.

Effects of Edge Blending on the Optical Response

Despite the advanced and sophisticated fabrication techniques employed to make nanoparticles, it is inevitable to have some variations in their geometrical shapes [48]. Clearly, such unintentional variations will cause discrepancies between the experimental data and the analytical or numerical predictions. For this reason, an analysis of possible deficiencies is essential to enhance the applicability of a theoretical model. To this end, we analyze in this section the effects of edge rounding on the extinction cross section and the field enhancement for hemispherical dimers. We focus on the case of parallel polarization and the edge-to-edge configuration since this case offers the most field enhancement and the largest extinction cross section.

Figure 9a shows changes in the peak-resonance frequency as a function of junction width for three values of the edge rounding radius a . With an increase in the blending, the resonance peak shifts to higher frequencies for similar gaps. The blending-induced blue shift for lowest separation is around 30 nm for $a = 3$ nm in comparison to sharp edge spectra. This shift increases to 50 nm for $a = 5$ nm. Several causes may be responsible for these shifts. First, when an edge is blended, the volume of the hemisphere is reduced, causing a reduction in number of electrons that may couple with the external field. As a result, the absorption and scattering cross sections are lower in hemispheres with blended edges [34]. Second, as a increases, the radius of hemispheres is also reduced, which enhances the oscillation strength of localized surface plasmons, which in turn results in a higher resonance frequency. Third, the spacing between the two hemispheres of a dimer gradually increases with edge rounding, resulting in a reduced interaction between the plasmon modes of two hemispheres [48]. The reduced attraction between nanoparticles results in a higher restoring force and the corresponding blue shift of the resonance frequency. Nevertheless, in accordance with the predictions of DDIM model, the plasmon resonance frequency of the nano-dimer with blended radii decreases

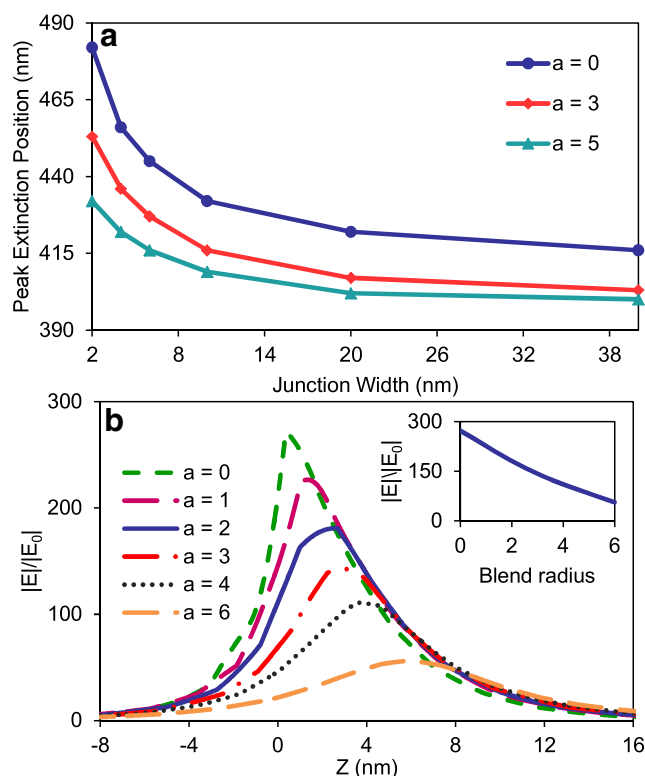


Fig. 9 Influence of edge rounding of hemispherical dimers on **a** extinction properties and **b** electric field enhancement. The inset of **b** illustrates the variation of field enhancement as a function of blend radii

exponentially as the spacing between the two hemispheres is reduced. For this reason, rounding of the edges does not affect the qualitative behavior of plasmon interaction in nano-hemispherical dimers. Figure 9b shows the impact of edge blending on the field enhancement factor by varying a from 0 to 6 nm. It is evident from the figure that increasing a causes a reduction in the SERS enhancement factor. Physically, a reduced localization of charges results in a change in hot-spot positions and a widening of the electric-field distribution in the vicinity of particles. From the inset of Fig. 9b, which shows how the maximum electric field enhancement along x - z plane is reduced with increasing blend radius a , we see that F_E decreases almost linearly with a for a hemispherical dimer. For example, F_E decreases from 227 to 111 as a increases from 1 to 4 nm.

Conclusions

In this paper, we have carried out a comprehensive study of the interaction of an electromagnetic wave with hemispherical nano-dimers. We discussed the dependency of optical response of such a nano-dimer on the dimer configuration, on the polarization direction of the incident field, and on the inter-hemisphere distance using an analytic description based on the dipole-dipole interaction and numerical simulations based on the FEM. More specifically, we first derived the polarization-dependant dipole moment of a single hemisphere invoking quasistatic theory and then employed the dipole-dipole interaction model (DDIM) to obtain polarizability of the nano-dimer. A comparison of the extinction spectra obtained from DDIM and numerical simulations reveals the competency of the analytical model in providing qualitative insight to the hybridization process of each hemispherical ensemble. However, for small inter-particle distances, charges of hemispheres lie in proximity, resulting in pronounced shifts in the frequency of plasmon resonances. Although DDIM estimations are fairly accurate for large spacings, they deviate considerably from numerical simulation when two hemispheres are brought closer. In addition, we found that the DDIM is inadequate for characterizing the orientation-dependent optical response of hemispheres placed side-by-side because of its use of the point-dipole approximation.

Our investigations show that extinction properties of a hemispherical nano-dimer and the extent of electric field enhancement vary considerably with the dimer configuration. Among the three configurations considered in this paper, the edge-to-edge orientation provides much better field enhancement in the junction region and much larger shifts of the resonance frequency when incident light is polarized parallel to the inter-hemisphere axis. Due to a larger displacement of surface plasmons in this arrangement

compared to side-by-side orientations, dipole moment is higher in the edge-to-edge orientation. Also, in the case of light polarization along the inter-hemisphere axis, plasmon modes of solitary particles lie closer compared to the case of transverse polarization, resulting in much stronger coupling. Nevertheless, transverse excitation of a D'-D ensemble results in better optical properties than the other two configuration when two hemispheres are closer due to the interaction of high-intensity electric fields along the edges of hemispheres. A comparison of field enhancement factors of hemispherical dimers with equal volume spherical dimers, in the case of edge-to-edge orientation and parallel polarization, reveals that it is possible to achieve quite large electric fields at the hot spots for the former, which makes this configuration more efficient for SERS applications. Moreover, rounding of hemisphere edges cause non-negligible effects on optical properties of hemispherical dimers. We found that for 20 nm radius hemisphere, the edge rounding resulted in a nearly linear drop of the electric field enhancement at the hot spots.

Acknowledgments The work of M. Premaratne and G. P. Agrawal is supported by the Australian Research Council through its Discovery Grants DP110100713 and DP140100883. T. Attanayake gratefully acknowledges financial support from Australian government and the Faculty of Engineering, Monash University.

References

1. Kreibig U, Vollmer M (1995) Optical properties of metal clusters. Springer
2. Mayer KM, Hafner JH (2011) Localized surface plasmon resonance sensors. *Chem Rev* 111(6):3828–3857
3. Sikdar D, Rukhlenko ID, Cheng W, Premaratne M (2013) Effect of number density on optimal design of gold nanoshells for plasmonic photothermal therapy. *Biomed Opt express* 4(1):15–31
4. Lal S, Link S, Halas NJ (2007) Nano-optics from sensing to waveguiding. *Nat Photonics* 1(11):641–648
5. Jain PK, Huang X, El-Sayed IH, El-Sayed MA (2007) Review of some interesting surface plasmon resonance-enhanced properties of noble metal nanoparticles and their applications to biosystems. *Plasmonics* 2(3):107–118
6. Sikdar D, Rukhlenko ID, Cheng W, Premaratne M (2013) Unveiling ultrasharp scattering-switching signatures of layered gold-dielectric-gold nanospheres. *J Opt Soc Am B* 30(8):2066–2074
7. Kumarasinghe C, Premaratne M, Agrawal GP (2014) Dielectric function of spherical dome shells with quantum size effects. *Opt Express* 22(10):11966–11984
8. Nordlander P, Oubre C, Prodan E, Li K, Stockman M (2004) Plasmon hybridization in nanoparticle dimers. *Nano Lett* 4(5):899–903
9. Bao K, Mirin NA, Nordlander P (2010) Fano resonances in planar silver nanosphere clusters. *Appl Phys A* 100(2):333–339
10. Averitt RD, Westcott SL, Halas NJ (1999) Linear optical properties of gold nanoshells. *J Opt Soc Am B* 16(10):1824–1832
11. Sikdar D, Rukhlenko ID, Cheng W, Premaratne M (2014) Tunable broadband optical responses of substrate-supported metal/dielectric/metal nanospheres. *Plasmonics* 9(3):659–672

12. Ljungbert A, Lundqvist S (1985) Non-local effects in the optical absorption of small metallic particles. *Surf Sci* 156:839–844
13. Chang R, Leung P (2006) Nonlocal effects on optical and molecular interactions with metallic nanoshells. *Phys Rev B* 73(12):125438–125444
14. David C, Garcia de Abajo FJ (2011) Spatial nonlocality in the optical response of metal nanoparticles. *J Phys Chem C* 115(40):19470–19475
15. Prodan E, Radloff C, Halas N, Nordlander P (2003) A hybridization model for the plasmon response of complex nanostructures. *Science* 302(5644):419–422
16. Jain PK, Eustis S, El-Sayed MA (2006) Plasmon coupling in nanorod assemblies: optical absorption, discrete dipole approximation simulation, and exciton-coupling model. *J Phys Chem B* 110(37):18243–18253
17. Fischer J, Vogel N, Mohammadi R, Butt HJ, Landfester K, Weiss CK, Kreiter M (2011) Plasmon hybridization and strong near-field enhancements in opposing nanocrescent dimers with tunable resonances. *Nanoscale* 3(11):4788–4797
18. Guerrero-Martínez A, Alonso-Gómez JL, Auguie B, Cid MM, Liz-Marzán LM (2011) From individual to collective chirality in metal nanoparticles. *Nano Today* 6(4):381–400
19. Zhao J, Pinchuk AO, McMahan JM, Li S, Ausman LK, Atkinson AL, Schatz GC (2008) Methods for describing the electromagnetic properties of silver and gold nanoparticles. *Acc Chem Res* 41(12):1710–1720
20. Oubre C, Nordlander P (2005) Finite-difference time-domain studies of the optical properties of nanoshell dimers. *J Phys Chem B* 109(20):10042–10051
21. Zhu S, Zhou W, Park GH, Li E (2010) Numerical design methods of nanostructure array for nanobiosensing. *Plasmonics* 5(3):267–271
22. Amendola V, Bakr OM, Stellacci F (2010) A study of the surface plasmon resonance of silver nanoparticles by the discrete dipole approximation method: effect of shape, size, structure, and assembly. *Plasmonics* 5(1):85–97
23. Aizpurua J, Rivacoba A, Apell S (1996) Electron-energy losses in hemispherical targets. *Phys Rev B* 54(4):2901–2909
24. Kettunen H, Wallén H, Sihvola A (2007) Polarizability of a dielectric hemisphere. *J Appl Phys* 102(4):044105–044112
25. Morse PM, Feshbach H (1953) *Methods of theoretical physics*
26. Kettunen H, Wallén H, Sihvola A (2008) Electrostatic resonances of a negative-permittivity hemisphere. *J Appl Phys* 103(9):094112–094120
27. Mayergoyz ID, Fredkin DR, Zhang Z (2005) Electrostatic (plasmon) resonances in nanoparticles. *Phys Rev B* 72(15):155412
28. Jain PK, El-Sayed MA (2010) Plasmonic coupling in noble metal nanostructures. *Chem Phys Lett* 487(4):153–164
29. Sheikholeslami S, Jun Yw, Jain PK, Alivisatos AP (2010) Coupling of optical resonances in a compositionally asymmetric plasmonic nanoparticle dimer. *Nano Lett* 10(7):2655–2660
30. Gomez D, Vernon K, Davis T (2010) Symmetry effects on the optical coupling between plasmonic nanoparticles with applications to hierarchical structures. *Phys Rev B* 81(7):075414
31. Sosa IO, Noguez C, Barrera RG (2003) Optical properties of metal nanoparticles with arbitrary shapes. *J Phys Chem B* 107(26):6269–6275
32. Weiland T, Timm M, Munteanu I (2008) A practical guide to 3-d simulation. *IEEE Microw Mag* 9(6):62–75
33. Palik ED (1998) *Handbook of optical constants of solids*, vol 3. Academic
34. Bohren CF, Huffman DR (2008) *Absorption and scattering of light by small particles*. Wiley
35. Esteban R, Borisov AG, Nordlander P, Aizpurua J (2012) Bridging quantum and classical plasmonics with a quantum-corrected model. *Nat Commun* 3:825
36. Hatab NA, Hsueh CH, Gaddis AL, Retterer ST, Li JH, Eres G, Zhang Z, Gu B (2010) Free-standing optical gold bowtie nanoantenna with variable gap size for enhanced raman spectroscopy. *Nano Lett* 10(12):4952–4955
37. Encina ER, Coronado EA (2010) Plasmon coupling in silver nanosphere pairs. *J Phys Chem C* 114(9):3918–3923
38. Brandl DW, Oubre C, Nordlander P (2005) Plasmon hybridization in nanoshell dimers. *J Chem Phys* 123(2):024,701
39. Rechberger W, Hohenau A, Leitner A, Krenn J, Lamprecht B, Aussenegg F (2003) Optical properties of two interacting gold nanoparticles. *Opt Commun* 220(1):137–141
40. Elghanian R, Storhoff JJ, Mucic RC, Letsinger RL, Mirkin CA (1997) Selective colorimetric detection of polynucleotides based on the distance-dependent optical properties of gold nanoparticles. *Science* 277(5329):1078–1081
41. Haes AJ, Hall WP, Chang L, Klein WL, Van Duyne RP (2004) A localized surface plasmon resonance biosensor: first steps toward an assay for Alzheimer's disease. *Nano Lett* 4(6):1029–1034
42. Unger A, Kreiter M (2009) Analyzing the performance of plasmonic resonators for dielectric sensing. *J Phys Chem C* 113(28):12,243–12,251
43. Haynes CL, McFarland AD, Duyne RPV (2005) Surface-enhanced raman spectroscopy. *Anal Chem* 77(17):338
44. Talley CE, Jackson JB, Oubre C, Grady NK, Hollars CW, Lane SM, Huser TR, Nordlander P, Halas NJ (2005) Surface-enhanced raman scattering from individual Au nanoparticles and nanoparticle dimer substrates. *Nano Lett* 5(8):1569–1574
45. Lu Y, Liu GL, Kim J, Mejia YX, Lee LP (2005) Nanophotonic crescent moon structures with sharp edge for ultrasensitive biomolecular detection by local electromagnetic field enhancement effect. *Nano Lett* 5(1):119–124
46. Sarid D, Challener W (2010) *Modern introduction to surface plasmons: theory, Mathematica modeling, and applications*. Cambridge University Press
47. Hao E, Schatz GC (2004) Electromagnetic fields around silver nanoparticles and dimers. *J Chem Phys* 120(1):357–366
48. Raziman T, Martin OJ (2013) Polarisation charges and scattering behaviour of realistically rounded plasmonic nanostructures. *Opt Express* 21(18):21,500–21,507